

Enhanced metal-insulator transition in freestanding VO₂ down to 5 nm thickness

Kun Han^{1,2, †}, Liang Wu^{1,3, † *}, Yu Cao^{4, †}, Hanyu Wang⁵, Chen Ye¹, Ke Huang¹, M. Motapothula^{6,7}, Hongna Xing⁸, Xinghua Li⁸, Dong-Chen Qi⁹, Xiao Li⁵, X. Renshaw Wang^{1,10,*}

¹*Division of Physics and Applied Physics, School of Physical and Mathematical Sciences, Nanyang Technological University, 21 Nanyang Link, 637371, Singapore*

²*Key Laboratory of Structure and Functional Regulation of Hybrid Materials of Ministry of Education, Institutes of Physical Science and Information Technology, Anhui University, Hefei 230601, China*

³*School of Material Science and Engineering, Kunming University of Science and Technology, Kunming, Yunnan 650093, China*

⁴*Department of Electrical and Computer Engineering, National University of Singapore, 4 Engineering Drive 3, Singapore 117583*

⁵*NNU-SULI Thermal Energy Research Center, Center for Quantum Transport and Thermal Energy Science (CQTES), School of Physics and Technology, Nanjing Normal University, Nanjing 210023, China*

⁶*Department of Physics and Astronomy, Uppsala University, Box 516, SE-75120 Uppsala, Sweden*

⁷*Department of Physics, SRM University AP, Amaravati, Andhra Pradesh 522-502, India*

⁸*School of Physics, Northwest University, Xi'an 710069, China*

⁹*Centre for Materials Science, School of Chemistry and Physics, Queensland University of Technology, Brisbane, QLD 4001, Australia*

¹⁰*School of Electrical and Electronic Engineering, Nanyang Technological University, 50 Nanyang Ave, 639798, Singapore*

†These authors contributed equally

*e-mail: liangwu@kust.edu.cn, renshaw@ntu.edu.sg

Keywords: Vanadium Dioxide, Metal-insulator transition, Freestanding membrane, Flexible electronics, Sr₃Al₂O₆

ABSTRACT

Ultrathin freestanding membranes with a pronounced metal-insulator transition (MIT) provides huge potential in future flexible electronic applications as well as a unique aspect of the study of lattice-electron interplay. However, the reduction of the thickness to an ultrathin region (a few nm) is typically detrimental to the MIT in epitaxial films, and even catastrophic for their freestanding form. Here, we report an enhanced MIT in VO₂-based freestanding membranes, with a lateral size up to millimetres and VO₂ thickness down to 5 nm. The VO₂-membranes were detached by dissolving a Sr₃Al₂O₆ sacrificial layer between the VO₂ thin film and *c*-Al₂O₃(0001) substrate, allowing a transfer onto arbitrary surfaces. Furthermore, the MIT in the VO₂-membrane was greatly enhanced by inserting an intermediate Al₂O₃ buffer layer. In comparison to the best available ultrathin VO₂-membranes, the enhancement of MIT is over 400% at 5 nm VO₂ thickness and more than one order of magnitude for VO₂ above 10 nm. Our study widens the spectrum of functionality in ultrathin and large-scale membranes, and enables the potential integration of MIT into flexible electronics and photonics.

INTRODUCTION

Metal-insulator transition (MIT), an appealing strongly correlated electronic phenomenon, offers switchable electronics states, which are ideal for future electronic and photonic applications¹. VO₂ is considered as one of the most attractive MIT materials, owing to its near room transition temperature (~341 K), where electrical conductivity can change up to six orders of magnitude²⁻³. Most recently, spurred by the technological interest for flexible electronics, such as flexible artificial neuron⁴⁻⁵ and low-power transistor⁶. It is of great demand to transform the MIT in VO₂ from a conventional epitaxial rigid form to a freestanding flexible one. Meaningful endeavours have achieved the VO₂-membranes (typically above 25 nm) using a number of techniques, including ion milling⁷, wet-etching based method⁸⁻¹⁰, or mechanical exfoliation from mica substrate¹¹. Furthermore, thanks to the continuous advancement of fabrication techniques, reducing the dimensions while retaining high-quality MIT in a flexible form can potentially lead to new insights into the interplays of lattice and electronic correlation¹² and utilization of flexible form of MIT in low-power flexible electronics. Hence, it is highly desirable to adopt a facile and gentle approach to preserve the MIT in freestanding large-scale VO₂ down to an

ultrathin region, *i.e.* below 10 nm^{7, 13}.

However, it is extremely challenging to obtain a freestanding ultrathin VO₂ membrane (< 10 nm) with high-quality MIT. This is due to a combination of several fundamental and technical issues, including the fundamental limit of critical thickness¹⁴, crystalline defects created during the fabrication¹³, and unwanted surface states introduced during the sample processing⁸⁻¹⁰. To date, only the complicated technique of ion milling⁷ managed to achieve a sub-20 nm VO₂-membranes by compromising the lateral size to tens of micrometres (limited by the growth approach) and a degraded MIT (due to ion-induced structural damages).

In this study, we demonstrate a facile fabrication to retain enhanced MIT in ultrathin and large-scale VO₂-membranes by utilizing an Al₂O₃ buffer layer and a water-soluble sacrificial Sr₃Al₂O₆ (SAO) layer^{12, 15-17}, albeit the underneath cubic SAO experiences a non-epitaxial growth on hexagonal *c*-Al₂O₃(0001) substrate. More importantly, by inserting an intermediate Al₂O₃ buffer layer between the SAO and VO₂ films, the millimetre-scale VO₂/Al₂O₃-membranes exhibit an enhanced MIT with the VO₂ thickness down to 5 nm. Quantitatively, this enhanced MIT is over 400% at 5 nm VO₂ thickness and more than one order of magnitude for VO₂ above 10 nm in comparison to the existing ultrathin VO₂-membranes⁷.

Experimental section

Sample fabrication

Single monoclinic (*M*)-phase VO₂ films with thickness from 4 to 120 nm were grown by pulsed laser deposition (PLD) on *c*-Al₂O₃ substrates with/without an SAO sacrificial layer and/or an Al₂O₃ buffer layer between them. During the deposition, the laser fluence was fixed at ~2 J/cm² with a repetition rate of 5 Hz. The growth temperature and oxygen partial pressure (*P*_{O₂}) for SAO and Al₂O₃ were 700 °C and 1 × 10⁻⁵ Torr, respectively. Then the temperature was decreased to 500 °C under the same *P*_{O₂}. VO₂ thin film was deposited at 500 °C with a *P*_{O₂} of 2 × 10⁻⁴ Torr. After deposition, the sample was *in situ* annealed at 500 °C with a *P*_{O₂} of 5 × 10⁻³ Torr for 1 h. Sequentially, the sample was cooled down to room temperature under the same *P*_{O₂}. Sintered polycrystalline SAO, Al₂O₃ ceramic pellets and a commercial vanadium single crystal were used as targets. The thickness was controlled by the number of the laser pulse, and

further calibrated by both stylus profilometer and X-ray reflectivity (see **Figure S1** in supporting information) Two types of heterostructure are fabricated, namely VO₂/SAO/*c*-Al₂O₃ and VO₂/Al₂O₃/SAO/*c*-Al₂O₃ heterostructures. As the SAO layer is dissolvable in deionized (DI) water^{15, 18}, immersing the heterostructures can detach the VO₂- or VO₂/Al₂O₃-membranes from the *c*-Al₂O₃ substrates, and get suspended in the DI water, which are ready to be transferred onto any arbitrary substrates. At last, in order to ensure a firm adhesion of the membranes onto the new surface of substrates, e.g. glass, the transferred membranes with the new substrates were annealed in a vacuum (< 10⁻⁶ Torr) at 120 °C for 1 h to remove the bubbles and residual water.

Characterization methods

The electrical transport properties were measured with a Quantum Design physical property measurement system (PPMS) in the temperature range from 300 to 400 K. X-ray diffraction (XRD) was performed on a Bruker D8 diffractometer equipped with a Cu K_{α1} source at a wavelength of 1.5406 Å operated at 40 keV and 40 mA in grazing incidence (GI) geometry. Raman spectra were performed in backscattering configuration and recorded at 532 nm laser excitation. The resolution for this configuration is 0.5 cm⁻¹.

RESULTS AND DISCUSSION

Figure 1 shows the deposition, detachment and transfer processes to achieve the VO₂ and VO₂/Al₂O₃ membranes. The MIT in VO₂ is accompanied by a structural phase transition from a low-temperature *M*-phase to a high-temperature rutile (*R*)-phase. **Figure 1** also shows optical images of the VO₂- and VO₂/Al₂O₃-membranes on glass substrates with a scale up to several millimetres.

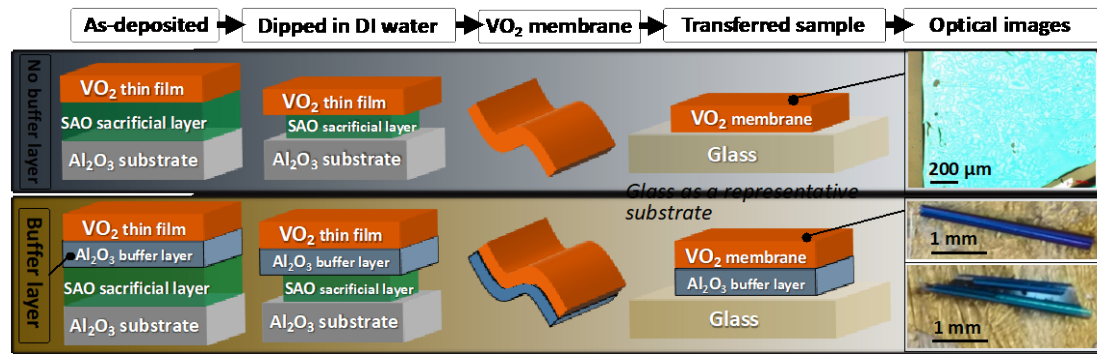


Figure 1. Schematics of the process to obtain ultrathin and large-scale VO₂ and VO₂/Al₂O₃ membranes. The as-grown samples, namely VO₂/SAO/c-Al₂O₃ and VO₂/Al₂O₃/SAO/c-Al₂O₃ heterostructures, are dipped in DI water to remove the SAO sacrificial layer. Consequently, ultrathin VO₂- and VO₂/Al₂O₃-membranes are achieved and can be transferred onto any substrates. In the schematics, glass substrates were used as a representative substrate. Eventually, optical images of the ultrathin and large-scale VO₂- and VO₂/Al₂O₃-membranes with a thickness down to 5 nm and a feature-length of mm are captured. The difference between these two types of membranes is the insertion of a buffer layer of Al₂O₃ during the growth.

It is worth mentioning that the efficiency of dissolving the SAO sacrificial layer is dramatically increased after inserting the Al₂O₃ buffer layer. The durations required for dissolving of the SAO layers in the 5 mm × 5 mm of VO₂/SAO/c-Al₂O₃ and VO₂/Al₂O₃/SAO/c-Al₂O₃ heterostructures are 1440 and 10 min, respectively. Moreover, the VO₂/Al₂O₃ membrane can be rolled into microtube during the dissolution of the SAO sacrificial layer in DI water without breaking, suggesting that the VO₂-membrane is highly flexible to bear a large degree of deformation. Specifically, the VO₂/Al₂O₃-membrane remains flat when the thickness of Al₂O₃ is below 10 nm and rolls up into a microtube for thicker Al₂O₃. The self-bending is ascribed to the low bending stiffness of the bilayer membrane system¹⁶ and unreleased strain between the Al₂O₃ and VO₂ layer.

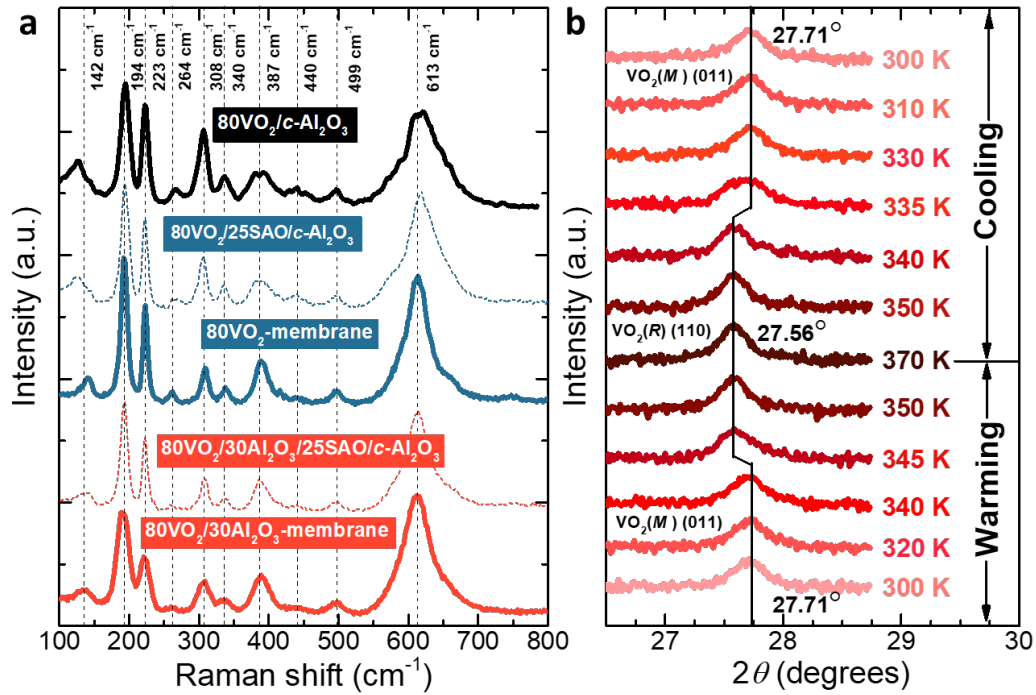


Figure 2. Structural characterisation of VO₂-based heterostructures and membranes. (a) Room temperature Raman spectra of 80VO₂/c-Al₂O₃, 80VO₂/25SAO/c-Al₂O₃, 80VO₂/30Al₂O₃/25SAO/c-Al₂O₃, 80VO₂-membrane, 80VO₂/30Al₂O₃-membrane. (b) Temperature-dependent HRXRD 2θ-ω scans of VO₂ (011) peak of the 80VO₂/30Al₂O₃/25SAO/c-Al₂O₃ at temperatures ranging from 300 to 370 K. The black arrow lines denote the peak shift across the MIT.

The structural phase of all the epitaxial films and membranes were firstly characterized by Raman spectroscopy with a 532 nm excitation laser source and temperature-dependent high-resolution X-ray diffraction (HRXRD). **Figure 2a** shows the room temperature Raman scattering curves for the 80 nm VO₂/c-Al₂O₃ heterostructure (abbreviated as 80VO₂/c-Al₂O₃, same notion will be used thereafter), 80VO₂/25SAO/c-Al₂O₃, 80VO₂-membrane, 80VO₂/30Al₂O₃/25SAO/c-Al₂O₃, and 80VO₂/30Al₂O₃-membrane. All the peaks at 194, 223, 264, 308, 340, 387, 440, 499, and 613 cm⁻¹ correspond to the pure *M*-phase VO₂ in both heterostructure and membrane forms at room temperature¹⁹. Moreover, the HRXRD measurement was conducted on VO₂/Al₂O₃/SAO/c-Al₂O₃ to confirm the thermal driven first-order SPT. **Figure 2b** shows that the VO₂(*M*) (011) peaks at 27.72° in the low-temperature region, *i.e.* from 300 to 340 K, shifts to rutile VO₂(*R*) (110) peaks at 27.58° in the high-

temperature region, *i.e.* from 345 to 370 K. When subsequently cooling the samples, the $\text{VO}_2(R)$ (110) peaks recover to the initial $\text{VO}_2(M)$ (011) peaks position²⁰⁻²¹. Therefore, both Raman and HRXRD results demonstrated that the crystallinity of the $\text{VO}_2(M)$ are well-retained when grown on SAO, and which is barely affected by the transfer process.

The electrical properties of the VO_2 heterostructures and membranes were characterized by the temperature-dependent resistivity and corresponding derivative curves, $d(\log\rho)/dT$. **Figure 3** shows that the MIT behaviour was preserved in all $\text{VO}_2/\text{SAO}/c\text{-Al}_2\text{O}_3$ samples, though the steepness of resistivity change is compromised and the magnitude of the resistivity change is suppressed in contrast to the epitaxial $\text{VO}_2/c\text{-Al}_2\text{O}_3$. The degraded MIT behaviour of $\text{VO}_2/\text{SAO}/c\text{-Al}_2\text{O}_3$ can be mainly attributed to the defects in VO_2 thin film induced by the SAO sacrificial layer. To overcome this, an Al_2O_3 buffer layer was inserted between VO_2 thin film and SAO sacrificial layer. **Figure 3a** shows that the resistivity change of $\text{VO}_2/\text{Al}_2\text{O}_3/\text{SAO}/c\text{-Al}_2\text{O}_3$ increases by around one order of magnitude and the MIT becomes much steeper. **Figure 3b** shows the normalized resistivity change, *i.e.* $\rho(T)/\rho(300\text{ K})$, as a function of temperature. Notably, the magnitude of the resistivity changes for $\text{VO}_2/\text{SAO}/c\text{-Al}_2\text{O}_3$ and VO_2 -membrane are comparable, as well as for $\text{VO}_2/\text{Al}_2\text{O}_3/\text{SAO}/c\text{-Al}_2\text{O}_3$ and $\text{VO}_2/\text{Al}_2\text{O}_3$ -membrane. The detailed comparison of MIT of different VO_2 can be found in **Table S1** in supporting information. The electrical transport measurements suggest that the influence of transferring procedure on its electrical transport properties is negligible.

To further characterize the change of MIT transition temperature (T_{MIT}) and the sharpness of resistivity change, several parameters are defined and plotted in **Figure 3c**. T_{Heat} and T_{Cool} are the specific transition temperature defined as the corresponding peak position of the derivative curves, $d(\log\rho)/dT$, during heating and cooling, respectively. Hence, T_{MIT} can be defined as $T_{\text{MIT}} = (T_{\text{Heat}} + T_{\text{Cool}})/2$. The hysteresis width (ΔH) is defined as the difference between T_{Heat} and T_{Cool} . The sharpness of the transition is defined as the full width at half maximum (FWHM) of the derivative curves during heating and cooling, which is derived by Gaussian fitting. **Figure 3c** shows that both T_{Heat} and T_{Cool} are slightly shifted towards room temperature for $\text{VO}_2/\text{SAO}/c\text{-Al}_2\text{O}_3$ and $\text{VO}_2/\text{Al}_2\text{O}_3/\text{SAO}/c\text{-Al}_2\text{O}_3$ and their corresponding membranes by comparing with that of $\text{VO}_2/c\text{-Al}_2\text{O}_3$. The decrease of T_{MIT} indicates VO_2 is compressively strained in both heterostructure and membranes forms by inserting the SAO sacrificial layer and

Al₂O₃ buffer layer^{9, 22}. The FWHM becomes much broader for VO₂/SAO/*c*-Al₂O₃ and VO₂/SAO-membrane, suggesting the degraded quality of VO₂¹⁰. After inserting an Al₂O₃ buffer layer between VO₂ and SAO, the resistivity change becomes sharper²³, which again proves the beneficial effect of buffer Al₂O₃.

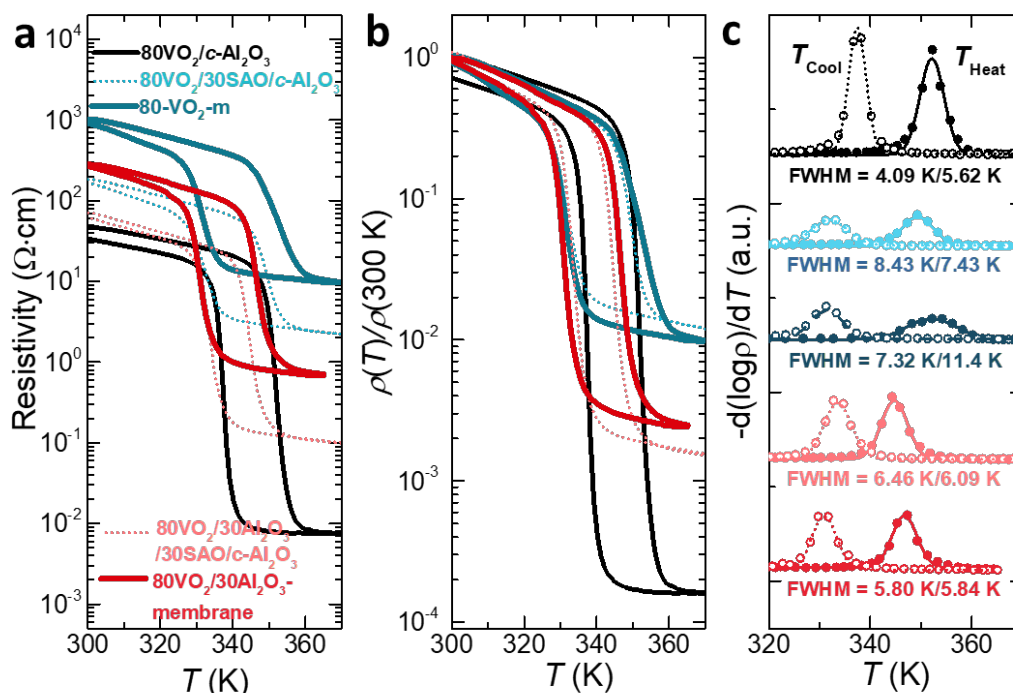


Figure 3. Effect of Al₂O₃ buffer layer. (a) Resistivity, (b) normalized resistivity changes, *i.e.* $\rho(T)/\rho(300\text{ K})$, and (c) derivatives of $\log_{10}\rho(T)$ as a function of temperature during the cooling (hollow circle) and heating (solid circle) cycles of the various VO₂-based heterostructures and membranes. The symbols and lines represent data points and Gaussian fitting curves, respectively.

The MIT properties of VO₂ are dramatically affected by thickness as well^{7, 24}. A minimum thickness is needed for the full development of the electronic MIT, such as the study of quantum confinement effects⁷. Therefore, an ultrathin VO₂ membrane is a prerequisite to have a deeper examination of the intrinsic MIT properties and quantum size effects. **Figure 4a-e** shows temperature-dependent resistivity of VO₂/*c*-Al₂O₃, VO₂/SAO/*c*-Al₂O₃, VO₂-membrane, VO₂/Al₂O₃/SAO/*c*-Al₂O₃, and VO₂/Al₂O₃-membrane with different VO₂ thicknesses. For all VO₂ films with thickness above 20 nm, the MIT properties are retained. It is worth noting that the critical thickness for MIT in VO₂ film increases from 4 nm for VO₂/*c*-Al₂O₃ to 15 nm for VO₂/SAO/*c*-Al₂O₃ and 20 nm

for VO₂-membrane, indicating that the VO₂ deteriorates when grown on SAO. Remarkably, the critical thickness recovers to 5 nm for VO₂/Al₂O₃/SAO/c-Al₂O₃ and corresponding VO₂/Al₂O₃-membrane, demonstrating that the quality of the VO₂ is comparable with that of VO₂ directly grown on c-Al₂O₃ substrate²⁵.

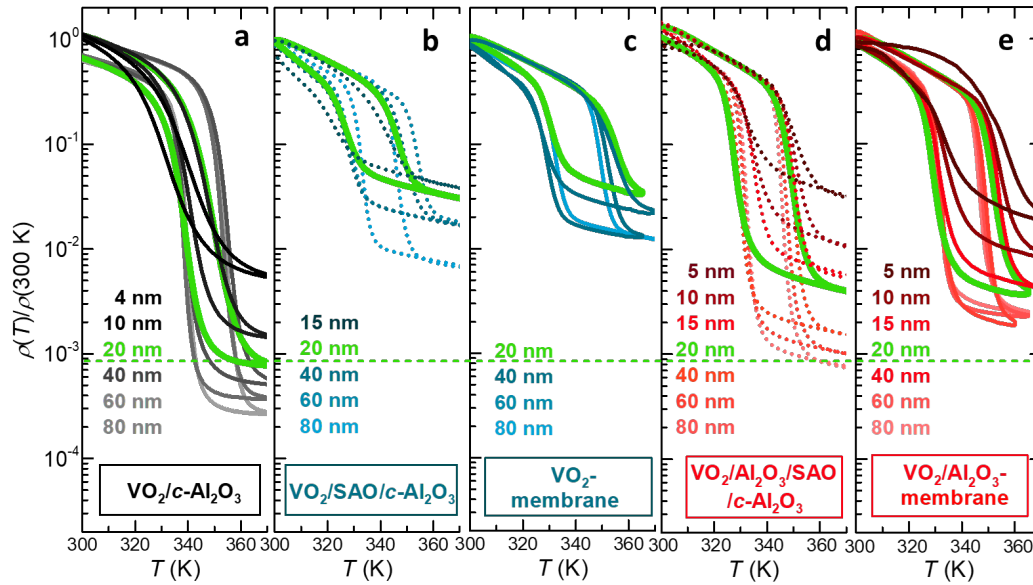


Figure 4. Thickness dependent metal-insulator transition of VO₂-based heterostructures and VO₂-membranes. Normalized resistivity change, *i.e.* $\rho(T)/\rho(300\text{ K})$, of (a) VO₂/c-Al₂O₃, (b) VO₂/SAO/c-Al₂O₃, (c) VO₂-membrane, (d) VO₂/Al₂O₃/SAO/c-Al₂O₃, and (e) VO₂/Al₂O₃-membrane. The labels of the thickness in all figures correspond to the VO₂ thicknesses in the respective samples.

Figure 5 compares the thickness dependence of the resistivity change across the MIT, $\rho(300\text{ K})/\rho(370\text{ K})$ of different ultrathin VO₂-membranes prepared in this work and the pioneer work in ref [7]. One can clearly see the magnitude of the resistivity change during the MIT in this study is over one order of magnitude better than the previous study for VO₂ above 10 nm, which can still be maintained to 400% when the thickness of VO₂ is reduced to 5 nm. In addition to the exceptional MIT, the water-soluble sacrificial SAO layer approach shows celebrated advantages in obtaining both large-scale, high-quality VO₂ membranes with an easy-handling process.

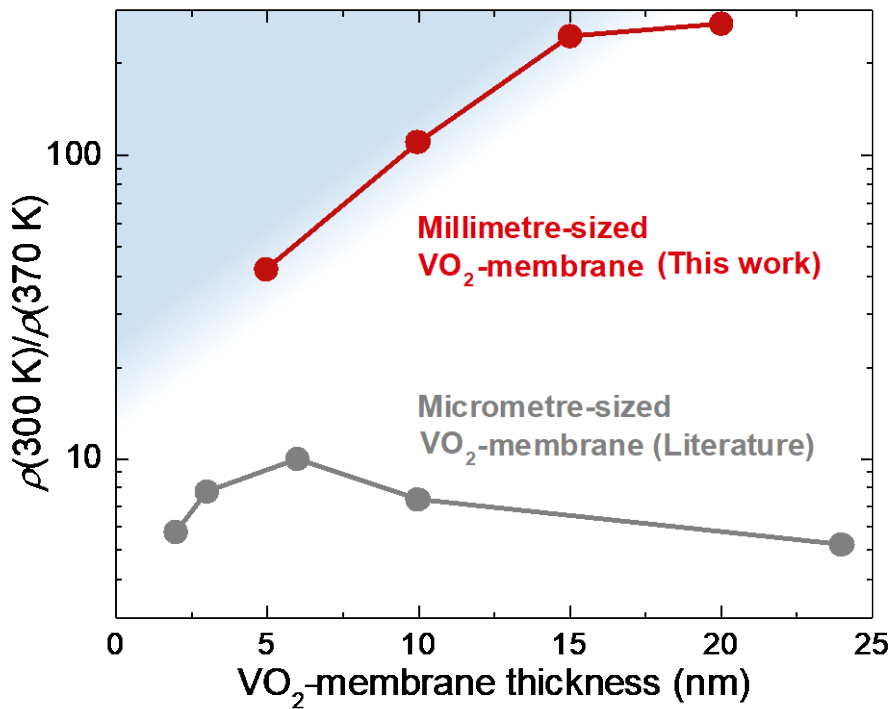


Figure 5. Comparison of the MIT in ultrathin VO₂-membranes (less than 25 nm) fabricated by different methods. The thickness dependence of the resistivity change, $\rho(300\text{ K})/\rho(370\text{ K})$, across the MIT of VO₂-membranes by different fabrication methods.

Conclusion

In summary, we have demonstrated a facile synthesis method to fabricate freestanding large-scale VO₂ ultrathin membranes by inserting SAO as a sacrificial layer and Al₂O₃ as a buffer layer between the VO₂ film and c-Al₂O₃ substrate. Both the *M*-phase crystal structure and the corresponding MIT behaviour are preserved in the VO₂- and VO₂/Al₂O₃-membranes form, albeit the SAO cannot be epitaxially grown on c-Al₂O₃ substrate. Furthermore, the MIT quality of the VO₂ membranes is notably improved by employing an Al₂O₃ buffer layer even for VO₂ down to 5 nm, which shows great advantages as compared with the previous studies and guarantees the excellent flexibility for future low-power flexible electronics. Our VO₂/Al₂O₃-membranes demonstrated advantages of the higher magnitude of the MIT resistivity change in a larger area and thinner VO₂-membranes than the VO₂-membranes prepared by other techniques. Our results could pave the way for practically and versatily integrating high-quality MIT in future flexible electronics and photonics.

Supporting Information

Detailed comparison of MIT of different VO₂ films (Table S1); Atomic force microscopy and X-ray reflectivity calibration of film thickness (Figure S1)

Acknowledgement

X.R.W. acknowledges supports from the Academic Research Fund Tier 1 (Grant No. RG177/18) from Singapore Ministry of Education, and the Singapore National Research Foundation (NRF) under the competitive Research Programs (CRP Grant No. NRF-CRP21-2018-0003), and Agency for Science, Technology and Research (A*STAR) under its AME IRG grant (Project No. A20E5c0094). D.Q. acknowledges the support of the Australian Research Council (Grant No. FT160100207) and the continued support from the Queensland University of Technology (QUT) through the Centre for Materials Science. K. H. acknowledges the support from Singapore National Research Foundation (NRF) under the Competitive Research Programs (CRP Award No. NRFCRP15-2015-01). We thank C. Yu, SW Zeng, Z. Huang, S. Goswami, A. Ariando and T. Venky Venkatasen on their fruitful discussion and help during the sample growth.

REFERENCES

- (1) Imada, M.; Fujimori, A.; Tokura, Y. Metal-Insulator Transitions. *Rev. Mod. Phys.* **1998**, *70* (4), 1039-1263.
- (2) Shao, Z.; Cao, X.; Luo, H.; Jin, P. Recent Progress in the Phase-Transition Mechanism and Modulation of Vanadium Dioxide Materials. *NPG Asia Mater.* **2018**, *10* (7), 581-605.
- (3) Liu, K.; Lee, S.; Yang, S.; Delaire, O.; Wu, J. Recent Progresses on Physics and Applications of Vanadium Dioxide. *Mater. Today* **2018**, *21* (8), 875-896.
- (4) Yi, W.; Tsang, K. K.; Lam, S. K.; Bai, X.; Crowell, J. A.; Flores, E. A. Biological Plausibility and Stochasticity in Scalable VO₂ Active Memristor Neurons. *Nat. Commun.* **2018**, *9* (1), 4661.
- (5) del Valle, J.; Salev, P.; Tesler, F.; Vargas, N. M.; Kalcheim, Y.; Wang, P.; Trastoy, J.; Lee, M.-H.; Kassabian, G.; Ramírez, J. G.; Rozenberg, M. J.; Schuller, I. K. Subthreshold Firing in Mott Nanodevices. *Nature* **2019**, *569* (7756), 388-392.
- (6) Shukla, N.; Thathachary, A. V.; Agrawal, A.; Paik, H.; Aziz, A.; Schlom, D. G.; Gupta, S. K.; Engel-Herbert, R.; Datta, S. A Steep-Slope Transistor Based on Abrupt Electronic Phase Transition. *Nat. Commun.* **2015**, *6* (1), 7812.
- (7) Fadlemula, M. M.; Sürmeli, E. C.; Ramezani, M.; Kasirga, T. S. Effects of Thickness on the Metal-Insulator Transition in Free-Standing Vanadium Dioxide Nanocrystals. *Nano Lett.* **2017**,

17 (3), 1762-1767.

(8) Tian, Z.; Xu, B.; Hsu, B.; Stan, L.; Yang, Z.; Mei, Y. Reconfigurable Vanadium Dioxide Nanomembranes and Microtubes with Controllable Phase Transition Temperatures. *Nano Lett.* **2018**, *18* (5), 3017-3023.

(9) Sim, J. S.; Zhou, Y.; Ramanathan, S. Suspended Sub-50 nm Vanadium Dioxide Membrane Transistors: Fabrication and Ionic Liquid Gating Studies. *Nanoscale* **2012**, *4* (22), 7056-62.

(10) Pellegrino, L.; Manca, N.; Kanki, T.; Tanaka, H.; Biasotti, M.; Bellingeri, E.; Siri, A. S.; Marre, D. Multistate Memory Devices Based on Free-Standing VO₂/TiO₂ Microstructures Driven by Joule Self-Heating. *Adv. Mater.* **2012**, *24* (21), 2929-34.

(11) Chen, Y.; Fan, L.; Fang, Q.; Xu, W.; Chen, S.; Zan, G.; Ren, H.; Song, L.; Zou, C. Free-Standing SWNTs/VO₂/Mica Hierarchical Films for High-Performance Thermochromic Devices. *Nano Energy* **2017**, *31*, 144-151.

(12) Hong, S. S.; Gu, M.; Verma, M.; Harbola, V.; Wang, B. Y.; Lu, D.; Vailionis, A.; Hikita, Y.; Pentcheva, R.; Rondinelli, J. M.; Hwang, H. Y. Extreme Tensile Strain States in La_{0.7}Ca_{0.3}MnO₃ Membranes. *Science* **2020**, *368* (6486), 71-76.

(13) Peter, A. P.; Martens, K.; Rampelberg, G.; Toeller, M.; Ablett, J. M.; Meersschant, J.; Cuypers, D.; Franquet, A.; Detavernier, C.; Rueff, J.-P.; Schaekers, M.; Van Elshocht, S.; Jurczak, M.; Adelman, C.; Radu, I. P. Metal-Insulator Transition in ALD VO₂ ultrathin Films and Nanoparticles: Morphological Control. *Adv. Funct. Mater.* **2015**, *25* (5), 679-686.

(14) Hong, S. S.; Yu, J. H.; Lu, D.; Marshall, A. F.; Hikita, Y.; Cui, Y.; Hwang, H. Y. Two-Dimensional Limit of Crystalline Order in Perovskite Membrane Films. *Sci. Adv.* **2017**, *3* (11), eaao5173.

(15) Lu, D.; Baek, D. J.; Hong, S. S.; Kourkoutis, L. F.; Hikita, Y.; Hwang, Harold Y. Synthesis of Freestanding Single-Crystal Perovskite Films and Heterostructures by Etching of Sacrificial Water-Soluble layers. *Nat. Mater.* **2016**, *15* (12), 1255-1260.

(16) Dong, G.; Li, S.; Yao, M.; Zhou, Z.; Zhang, Y. Q.; Han, X.; Luo, Z.; Yao, J.; Peng, B.; Hu, Z.; Huang, H.; Jia, T.; Li, J.; Ren, W.; Ye, Z. G.; Ding, X.; Sun, J.; Nan, C. W.; Chen, L. Q.; Li, J.; Liu, M. Super-Elastic Ferroelectric Single-Crystal Membrane with Continuous Electric Dipole Rotation. *Science* **2019**, *366* (6464), 475-479.

(17) Ji, D.; Cai, S.; Paudel, T. R.; Sun, H.; Zhang, C.; Han, L.; Wei, Y.; Zang, Y.; Gu, M.; Zhang, Y.; Gao, W.; Huan, H.; Guo, W.; Wu, D.; Gu, Z.; Tsymbal, E. Y.; Wang, P.; Nie, Y.; Pan, X. Freestanding Crystalline Oxide Perovskites Down to the Monolayer Limit. *Nature* **2019**, *570* (7759), 87-90.

(18) Han, K.; Hu, K.; Li, X.; Huang, K.; Huang, Z.; Zeng, S.; Qi, D.; Ye, C.; Yang, J.; Xu, H.; Ariando, A.; Yi, J.; Lu, W.; Yan, S.; Wang, X. R. Erasable and Recreatable Two-Dimensional Electron Gas at the Heterointerface of SrTiO₃ and a Water-Dissolvable Overlayer. *Sci. Adv.* **2019**, *5* (8), eaaw7286.

(19) Chen, F. H.; Fan, L. L.; Chen, S.; Liao, G. M.; Chen, Y. L.; Wu, P.; Song, L.; Zou, C. W.; Wu, Z. Y. Control of the Metal-Insulator Transition in VO₂ Epitaxial Film by Modifying Carrier Density. *ACS Appl. Mater. Interfaces* **2015**, *7* (12), 6875-81.

(20) Hada, M.; Okimura, K.; Matsuo, J. Characterization of Structural Dynamics of VO₂ Thin Film on c-Al₂O₃ Using in-Air Time-Resolved X-Ray Diffraction. *Phys. Rev. B* **2010**, *82* (15), 153401.

(21) Yang, M.; Yang, Y.; Wang, L.; Hong, B.; Huang, H.; Hu, X.; Zhao, Y.; Dong, Y.; Li, X.; Lu,

Y.; Bao, J.; Luo, Z.; Gao, C. For Progress in Natural Science: Materials International Investigations of Structural Phase Transformation and THz Properties across Metal–Insulator Transition in VO₂/ Al₂O₃ Epitaxial Films. *Prog. Nat. Sci-Mater* **2015**, *25* (5), 386-391.

(22) Muraoka, Y.; Hiroi, Z. Metal–Insulator Transition of VO₂ Thin Films Grown on TiO₂ (001) and (110) Substrates. *Appl. Phys. Lett.* **2002**, *80* (4), 583-585.

(23) Lee, D.; Lee, J.; Song, K.; Xue, F.; Choi, S. Y.; Ma, Y.; Podkaminer, J.; Liu, D.; Liu, S. C.; Chung, B.; Fan, W.; Cho, S. J.; Zhou, W.; Lee, J.; Chen, L. Q.; Oh, S. H.; Ma, Z.; Eom, C. B. Sharpened VO₂ Phase Transition Via Controlled Release of Epitaxial Strain. *Nano Lett* **2017**, *17* (9), 5614-5619.

(24) Yamin, T.; Wissberg, S.; Cohen, H.; Cohen-Taguri, G.; Sharoni, A. Ultrathin Films of VO₂ on r-Cut Sapphire Achieved by Postdeposition Etching. *ACS Appl. Mater. Interfaces* **2016**, *8* (23), 14863-70.

(25) Zhang, H.-T.; Zhang, L.; Mukherjee, D.; Zheng, Y.-X.; Haislmaier, R. C.; Alem, N.; Engel-Herbert, R. Wafer-Scale Growth of VO₂ Thin Films Using a Combinatorial Approach. *Nat. Commun.* **2015**, *6* (1), 8475.

Supporting Information

Enhanced metal-insulator transition in freestanding VO₂ down to 5 nm thickness

Kun Han^{1,2, †}, Liang Wu^{1,3, † *}, Yu Cao^{4, †}, Hanyu Wang⁵, Chen Ye¹, Ke Huang¹, M. Motapothula^{6,7}, Hongna Xing⁸, Xinghua Li⁸, Dong-Chen Qi⁹, Xiao Li⁵, X. Renshaw Wang^{1,10,*}

¹*Division of Physics and Applied Physics, School of Physical and Mathematical Sciences, Nanyang Technological University, 21 Nanyang Link, 637371, Singapore*

²*Key Laboratory of Structure and Functional Regulation of Hybrid Materials of Ministry of Education, Institutes of Physical Science and Information Technology, Anhui University, Hefei 230601, China*

³*School of Material Science and Engineering, Kunming University of Science and Technology, Kunming, Yunnan 650093, China*

⁴*Department of Electrical and Computer Engineering, National University of Singapore, 4 Engineering Drive 3, Singapore 117583*

⁵*NNU-SULI Thermal Energy Research Center, Center for Quantum Transport and Thermal Energy Science (CQTES), School of Physics and Technology, Nanjing Normal University, Nanjing 210023, China*

⁶*Department of Physics and Astronomy, Uppsala University, Box 516, SE-75120 Uppsala, Sweden*

⁷*Department of Physics, SRM University AP, Amaravati, Andhra Pradesh 522-502, India*

⁸*School of Physics, Northwest University, Xi'an 710069, China*

⁹*Centre for Materials Science, School of Chemistry and Physics, Queensland University of Technology, Brisbane, QLD 4001, Australia*

¹⁰*School of Electrical and Electronic Engineering, Nanyang Technological University, 50 Nanyang Ave, 639798, Singapore*

†These authors contributed equally

*e-mail: liangwu@kust.edu.cn, renshaw@ntu.edu.sg

Table S1

To quantitatively evaluate the quality of our VO₂ films and membranes, several key parameters are defined and listed in **Table S1**.

	ΔA	T_{heat} (K)	T_{cool} (K)	T_{MIT} (K)	ΔH (K)	ΔT (K)
VO ₂ /c-Al ₂ O ₃	6223	352.3	337.2	344.8	15.1	4.9
VO ₂ /SAO/c-Al ₂ O ₃	138	345.9	333.2	339.6	12.7	7.4
VO ₂ -membrane	83	349.2	332.2	340.7	17	7.2
VO ₂ /Al ₂ O ₃ /SAO/c-Al ₂ O ₃	1238	345.8	332.5	339.2	13.3	5.2
VO ₂ /Al ₂ O ₃ -membrane	409	347	331	339	16	5.4

ΔA : $(R(300K)/R(370K))$;

$T_{\text{MIT}} = (T_{\text{heat}} + T_{\text{cool}})/2$;

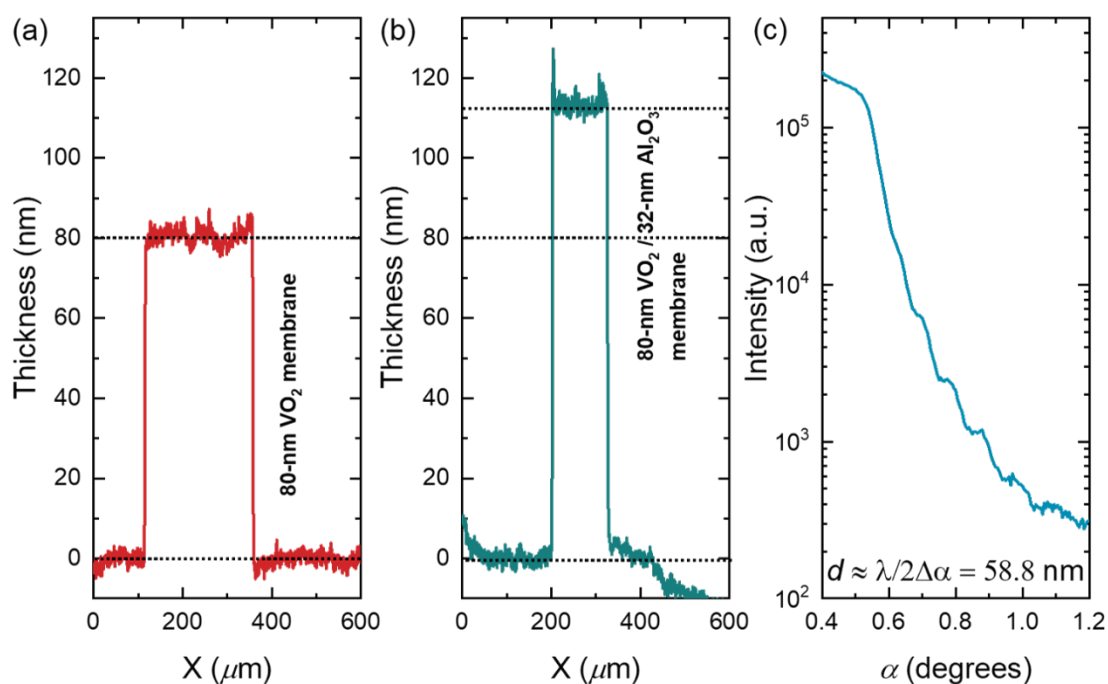
T_{heat} and T_{cool} : the transition temperatures defined as the peak position of the derivative curves ($d(\log\rho)/dT$) during heating and cooling.

ΔH : The hysteresis width is defined $\Delta H = T_{\text{heat}} - T_{\text{cool}}$;

ΔT : The sharpness of the transition, which is defined as the FWHM of the derivative curve during heating.

Figure S1

The thickness of VO₂ films is calibrated by results of profilometry (**Figure S1a,b**) and X-ray reflectivity (**Figure S1c**). Both results are consistent, which provides the thickness controlling by counting the number of the laser pulse. For VO₂, 1 nm corresponds to 500 pulses; For Al₂O₃, 1 nm corresponds to 20 pulses.



Supplementary Figure S1. Thickness calibration of different VO₂. The thicknesses of (a) 40000 pulses VO₂-membrane and (b) 40000 pulses VO₂/600 pulses Al₂O₃ were measured by Bruker profilometer. (c) The X-ray reflectivity (XRR) of 30000 pulses VO₂/c-Al₂O₃ heterostructure. The thickness of the VO₂ film obtained by fitting is 58.8 nm. The thicknesses measured by both methods are consistent. All the thicknesses used in this study are calibrated by the laser pulses.